Journal of Ultrafine Grained and Nanostructured Materials
https://jufgnsm.ut.ac.ir
Vol. 57, No.1, June 2024, pp. 82-91
Print ISSN: 2423-6845 Online ISSN: 2423-6837
DOI: 10.22059/jufgnsm.2024.01.10

Thermoelectric Performance of Annealed SnSe/Bi_2Te_3 Bilayer and Multilayer Thin Films Prepared by Physical Vapor Deposition

Tamilarasi R[1], Magesh R[1], Joelin C[1], Suryakanth J[2],Rajesh S[*,1]

[1]Department of Physical Sciences, Karunya Institute of Technology and Sciences, Coimbatore 641 114, Tamil Nadu, India;
[2]Department of Physics, KPR Institute of Engineering and Technology, Coimbatore 641 407, Tamil Nadu, India.

Recieved: 11 February 2024; Accepted: 13 June 2024

**Corresponding author email: drsrajesh@karunya.edu*

ABSTRACT

Thermoelectrics are critical for sustainable energy development because they allow for the direct conversion of waste heat into electricity, improve energy efficiency in a variety of applications, and provide a clean, dependable, and maintenance-free alternative for power generation. In recent days, metal chalcogenides have gained more attention in the field of thermoelectrics. Among the chalcogenide materials, Tin Selenide is a promising material for mid-temperature thermoelectric applications, whereas Bismuth Telluride is mainly known for its room-temperature thermoelectric applications. The combination of these two materials would probably enhance the performance of the thermoelectric generator. The present work deals with bilayer and multilayer thin film deposition of Tin Selenide and Bismuth Telluride on the glass substrates by physical vapor deposition. Then the deposited thin films were given a post-annealing treatment for 30 minutes at 323 K, 423 K, and 523 K. The structure and morphology of the thin films have been studied using X-Ray Diffraction (XRD), Scanning Electron Microscopy(SEM), Field Emission Scanning Electron Microscopy(FE-SEM) and Atomic Force Microscopy (AFM). The Seebeck Coefficient and Electrical conductivity of the bilayer and multilayer thin films were studied using the Seebeck Coefficient measurement system as temperature as function in a range of 300K to 573 K. The maximum Seebeck Coefficent of -350µV/K was obtained for both bilayer and multilayer thin film at 573 K. The highest electrical conductivity of 220S/m and 170S/m were obtained for bilayer and multilayer thin film respectively. The power factor that gives the thermoelectric generator's performance was calculated from the Seebeck Coefficient and Electrical conductivity. The overall power factor for 573 K annealed films of bilayer and multilayer thin films increases with rise in temperature. The maximum obtained power factor for bilayer and multilayer thin films were 25W/K^2m and 18 W/K^2m respectively. An increase in the annealing temperature leads to improved thermoelectric performance for both bilayer and multilayer thin films.

Keywords: *Electrical Conductivity, Physical Vapor Deposition, Seebeck Coefficient, Thermoelectric, Thin films, Tin Selenide, Bismuth Telluride, Annealing.*

1. Introduction

Thermoelectricity is defined as the conversion of heat flow or temperature difference into useful electrical energy [1–4]. The performances of thermoelectric devices are given by Dimensionless Figure of Merit (ZT). The Figure of merit was determined by Seebeck Coefficient (S), Electrical Conductivity (σ) and Thermal Conductivity (k). The thermal conductivity has to components one is Electrical thermal Conductivity (k_e) and other is lattice thermal Conductivity (k_l) [5–8]. Electric thermal conductivity is related to electrical conductivity by Weidmann Franz law [9]. Because electric thermal conductivity is tied to electrical conductivity, re-

ducing it will also diminish the material's electrical conductivity, compromising the systems total ZT value [10]. In semiconductors, lattice thermal conductivity, which was unrelated to electrical conductivity, contributes more than 90% of the overall thermal conductivity [11]. The product of Seebeck Co efficient and Electrical Conductivity was known to be Power Factor [11]. The power factor should be maximized while thermal conductivity should be minimized for high ZT value [11, 13].

ZT values appear to be limited in bulk thermoelectric materials. However, advances in thin film technology have improved the ZT value of thermoelectric materials by nanostructuring [14]. Nanostructures provide greater thermoelectric performance due to higher thermal boundary resistances than electrical boundary resistances. Lattice reduction of the k_l component of heat conductivity causes the k_e/k ratio to increase. This may result in greater ZT values for nanostructured materials compared to bulk values, which has lately been a prominent topic of thermoelectric study [15, 16]. The desired nanostructures can change the phonon and electron transport characteristics of thermoelectric materials. Since L. D. Hicks and M. S. Dresselhaus asserted that the low dimensionality of quantum excellent superlattice materials can significantly improve the ZT value, the investigation of TE thin films has been encouraged for modern micro-thermoelectric devices [17]. Thin film technology was a good technique for improving the thermoelectric characteristics of materials because of the increased quantum confinement effect [18].

In recent research, compounds from the IVA, VA, and VIA groups have been identified as the best thermoelectric materials. The thermoelectric field has extensively explored these materials, including Sn(S, Se, Te), Pb (S, Se, Te), Ge (S, Se, Te), Bi_2Te_3, Sb_2Te_3, and their related alloys [15].Tin Selenide (SnSe) has long been recognized as material for mid-temperature applications due to its second-order reverse phase transition at temperature ranging from 750K to 800K [12]. In 2014 Zhou et al. reported that the ZT value of a single-layered SnSe crystal was 2.6 at 973 K [16]. Similarly, Bismuth Telluride Bi_2Te_3 is a good candidate for room-temperature applications [17]. In 2011, Saleemi et al. achieved ZT value of 1.1 for undoped Bi_2Te_3 at 340K [18]. In 2015, Lipeng Hu et al. worked on Bi_2Te_3alloy and achieved ZT value of 1.2 at 357K [19]. The ZT value of 0.21 at 719K was obtained for 6% Bi doped SnSe nanosheets in 2018 by Chandra et al. [20]. In 2020 Ju et al obtained enhanced ZT value of Te nanoneedle/SnSe composites which was 3.2 times greater than pristine SnSe [21]. Bi_2Te_3exhibits a high thermoelectric Fig. of merit (ZT), as does SnSe[22–24]. At high temperatures, SnSe in particular shows very high ZT values, but Bi_2Te_3functions well at typical temperatures. SnSe is a great thermoelectric material because of its high Seebeck coefficient and low heat conductivity[25]. Bi_2Te_3 is well-known for having a respectable Seebeck coefficient and strong electrical conductivity[26]. It could potentially be possible to get a wide temperature range of excellent performance by combining these materials. The current study compares the thermoelectric performance of bilayer and multilayer SnSe/ Bi_2Te_3 thin films.

Material's surfaces act as an interface between the material and its surroundings, influencing a wide range of physical and chemical interactions. The deposition of a thin film onto a substrate modifies the surface in ways that can enhance or tailor the material's performance for specific applications. In thermoelectric applications, the surface qualities determine the material's capacity to convert heat to electrical energy. Thorough engineering and surface characterization are necessary to improve thermoelectric thin film stability, efficiency, and lifetime [27].

Most of the thin film deposition methods have been proposed for SnSe and Bi_2Te_3. They are DC Sputtering [24,28], RF Sputtering [29], Pulsed Laser Deposition (PLD) [30], Thermal Evaporation [5,25,26] and Electro deposition [23,27,28]. Among these techniques, Thermal evaporation is a promising one for metal chalcogenides with vacuum-based technology. Also. it is possible to deposit a single or can be multiple materials in a layered structure. Thermal evaporation is the process of heating a solid substance in a high vacuum chamber to a temperature that creates vapor pressure. A variety of sources are used to evaporate materials depending on whether they are available in wire, foil, ingot or powder form. Molybdenum boat which can withstand high temperature without reacting with the source material is used to hold the source material. A vapor cloud might form within the chamber due to the comparatively low pressure inside the vacuum. This evaporated substance is now vapor steam, which travels through the chamber and strikes the substrate, adhering to it as a coating or film. Quartz crystal thickness monitors, also known as digital thickness monitors

(DTM), were used to measure the thickness and rate of deposition. Inside the vacuum chamber, a quartz crystal arrangement that can be adjusted near to the substrates is installed. It is critical to understand this crystal's working frequency range and electrode quality. An electric monitor outside the chamber generates a current that causes the crystal to vibrate and measures the frequency over time. It is critical that this monitor reliably tracks crystal frequency variations and temperature characteristics. These frequency variations in time can be converted to the actual thickness of the film by an inbuilt microprocessor. Although thermal evaporation provides many advantages, there are limitations. Not all materials are suitable for evaporation; they are unsuited for coating surfaces with complicated topographies, and maintaining the right stoichiometry in compound materials can be challenging since various elements have different vapor pressures and evaporation rates.

2. Experimental

A glass is used as a substrate. The use of glass substrates in the synthesis of thermoelectric thin films provides thermal stability, a smooth surface to produce uniform films, and electrical insulation to prevent unwanted electrical conduction that could interfere with the thermoelectric device's function. The glass substrates were cleaned ultrasonically in soap water, ethanol, deionized water, and acetone for 30 minutes respectively. Then the substrates were arranged in a substrate holder and placed in the vacuum chamber. The source materials SnSe (Alfa Aesar 99.999% metals basis) and Bi_2Te_3 (Alfa Aesar 99.999% metals basis) were taken in molybdenum boats separately. The base pressure was created by rotary pump while high pressure was maintained by diffusion pump to get contamination free deposition. The pressure in the chamber was monitored using Pirani Gauge and Penning Gauge respectively. The high vacuum of 3 x 10-5 torr was maintained in the vacuum chamber. The digital thickness monitor (DTM) measures the thickness of the deposited film. The deposition rate is controlled by heating power and also monitored in DTM. Fig. 1 shows the schematic representation

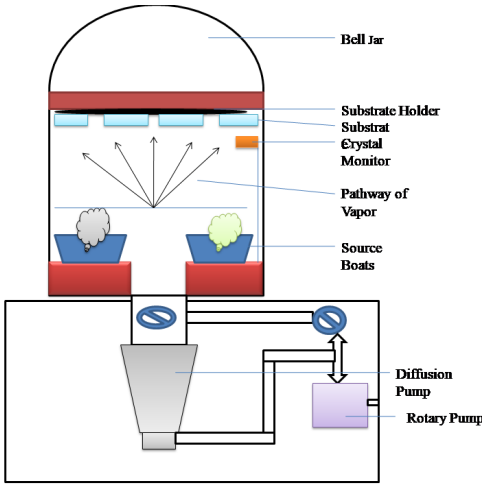

Fig. 1- Schematic Representation of two source physical evaporation.

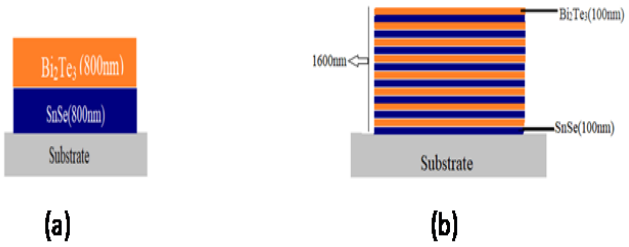

Fig. 2- Schematic diagrams of SnSe/ Bi2Te3 (a) bilayer (b) multilayer thin films.

of dual source physical evaporation unit. For bilayer deposition, first SnSe was deposited with a thickness of 800 nm and then Bi_2Te_3 was deposited with a thickness of 800 nm. For multilayer deposition, the SnSe and Bi_2Te_3 were deposited alternatively with 100 nm thickness of each for 8 periods. The overall thickness of the bilayer and multilayer films was 1600 nm. Fig. 2 shows the schematic diagram of the deposited bilayer and multilayer thin films. The deposited films were given a post-annealing treatment for 30 minutes at 323 K, 423 K, and 523 K respectively.

The Structural properties of the annealed bilayer and multilayer thin films have been studied using Cu Kα radiation (Shimadzu XRD-6000) diffraction ranging from 10˚- 80˚ with step size of 0.02. The surface morphology of the thin films was studied using Scanning Electron Microscope (SEM- Jeol), Field Emission Electron Microscope (Zeiss FESEM Sigma VP 03-04) and Atomic Force Microscope (Flex – Axiom AFM). The Hall Effect of the thin films was analyzed using hall effect measurement system (HMS 7000, Ecopia, South Korea). The Seebeck coefficient and electrical conductivity of the thin films were measured simultaneously as a function of temperature by the Seebeck coefficient measurement system (Marine India Seebeck Measurement system –SM800).The Fig. 3 (a) Module of thermoelectric measurement. The Seebeck measurement is a way to gauge how much of a thermoelectric voltage is created by the Seebeck effect in response to a temperature difference across a material. To maintain a correct heat gradient over the material, the test is conducted in a vacuum. Low to high voltage across the sample is measured using a high resolution Keithley multimeter. The Seebeck Coefficient measurement was measured from ambient temperature to 573 K. Fig.3 (b) Representation of Seebeck Coefficient measurement system.

3. Result and Discussion

3.1. Structure and Morphology

Fig. 4 (a) shows the X-ray diffraction pattern of bilayer thin films of SnSe/ Bi_2Te_3 at various anneal-

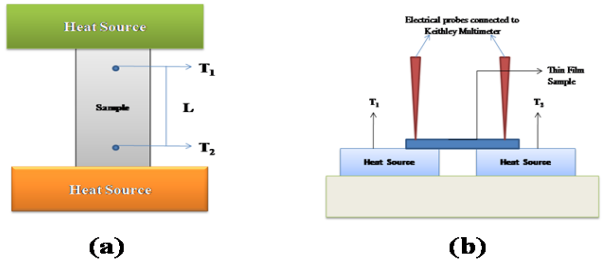

Fig. 3- (a) Module of thermoelectric Measurement (b) A schematic showing the Seebeck measurement set up.

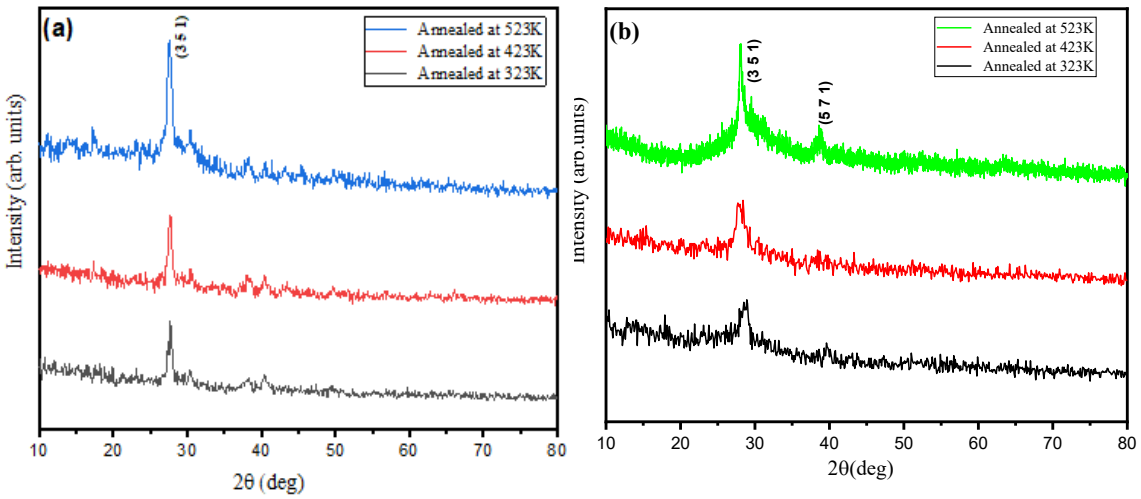

Fig. 4- X-Ray Spectrum of (a) Bilayer and (b) Mulilayer thin films at various annealing temperatures.

ing temperatures and Fig. 4 (b) shows the X-ray diffraction pattern multilayer thin films of SnSe/ Bi_2Te_3 at various annealing temperatures. The Fig. 4 (a) and (b) clearly shows as the annealing temperature increases, the crystallinity of both the bilayer and multilayer thin films increases. Every peak in the bilayer and multilayer thin films corresponds to the JCPDS card (#491380). Both bilayer and multilayer films have a sharp peak at $2\theta = 28.05°$, corresponding to (3, 1, 5) hkl values. There is an additional peak in the multilayer thin film, which was annealed at 523 K at 40°, corresponding to (5, 7, 1) hkl values. The crystallite sizes of all the films were calculated using Scherers' equation $D = 0.94\lambda/\beta\cos\theta$, where λ is the wavelength of the X-ray beam (Cukα =1.54Å), 2θ is the angle between the incident and scattered X-ray beam and β is the full width at half maximum [35]. The crystallite sizes of the bilayer thin films annealed at 323 K, 423 K, and 523 K were 11.08nm, 12.61nm, and 13.69nm, respectively. Similarly, the crystallite sizes at 323 K, 423 K, and 523 K annealed multilayer thin films were 5.6nm, 7.21nm, and 15.48nm, respectively. As the annealing temperature rises, the grain size of both the bilayer and multilayer thin films tends to increase and the peaks are getting sharper with high intensity. This indicates the change in phase structure of the coatings. The annealing temperature raises the kinetic energy of the atoms and molecules in the material, increasing their mobility. Grain boundary migration and other activities are made easier by the atoms' increased mobility due to this improved diffusion [7,36]. The average crystallite size rises as a result of smaller crystallites' propensity to combine or coalesce. The morphology of the thin films had been studied by SEM and FESEM. Fig. 5 (a), (b) and (c) shows the top viewed SEM image bilayer thin films annealed at 323 K, 423 K and 523 K respectively and Fig. 5(d), (e) and (f) shows the top viewed SEM image multilayer thin films annealed at 323 K, 423 K and 523 K respectively. From all images of Fig. 5 it is clear that uniform grains are spread over the surface of the thin film. The grains of the deposited thin film were unevenly distributed for both bilayer and multilayer samples annealed at 323 K. Although the surface morphology of the grains did not change noticeably after annealing at 423 K and 523 K, the grains did enlarge with rising annealing temperatures. Due to the post-annealing treatment, there is a minor modulation in the morphology and grain size of the thin films. To confirm the bilayer and multilayer formation the cross-sectional FESEM was carried out. The cross-sectional FESEM image of the bilayer and multilayer thin films annealed at room temperature was shown in Fig. 6. Fig. 6(a) shows the bilayer formation of SnSe/ Bi_2Te_3, and the multilayer formation of the thin films was shown in Fig. 6 (b). This shows the adhesion of the thin films to the substrates. The surface roughness of the bilayer and multilayer thin were studies using AFM. The AFM images of bilayer and multilayer thin films annealed at 323 K, 423 K and 523 K were shown in Fig. 7(a) - (f) respectively. As the annealing temperature increases there is a uniform grains seen on the surface of thin film. The

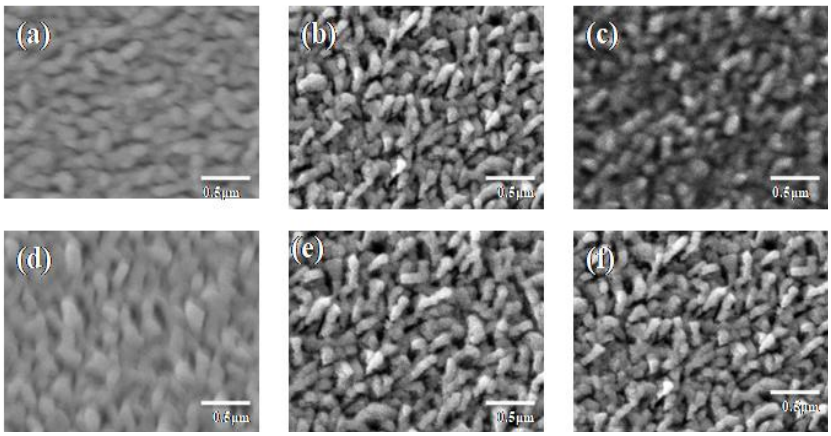

Fig. 5- Surface morphology through SEM image of bilayer thin films (a) annealed at 323 K (b) annealed at 423 K and (c) annealed at 523 K and multilayer thin films (d) annealed 323 K (e) annealed at 423 K and (f) annealed at 523 K.

average surface roughness (S_a) and the root mean square roughness (S_q) of the bilayer and multilayer thin film annealed at different temperatures were calculated using Gwyddion software. The average surface roughness (S_a) of the bilayer thin films annealed at 323 K, 423 K and 523 K were 176.98nm, 140.63nm and 123.712nm and the root mean square roughness (S_q) were 47.42nm, 42.02nm and

Table 1- Crystallite Size and Surface roughness of Bilayer and Multilayer thin films annealed at different temperatures

Thin Film	Annealing Temperature (K)	Crystallite Size (nm)	Surface Roughness(S_a) (nm)
Bilayer	323	11.08	176.98
	423	12.61	140.63
	523	13.69	123.712
Multilayer	323	5.6	81.71
	423	7.21	66.77
	523	15.48	56.85

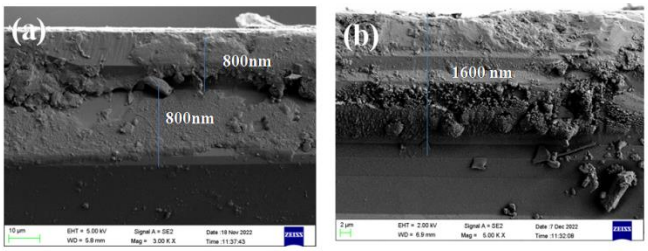

Fig. 6- Cross sectional FESEM (a) Bilayer Thin film (b) Multilayer Thin Film.

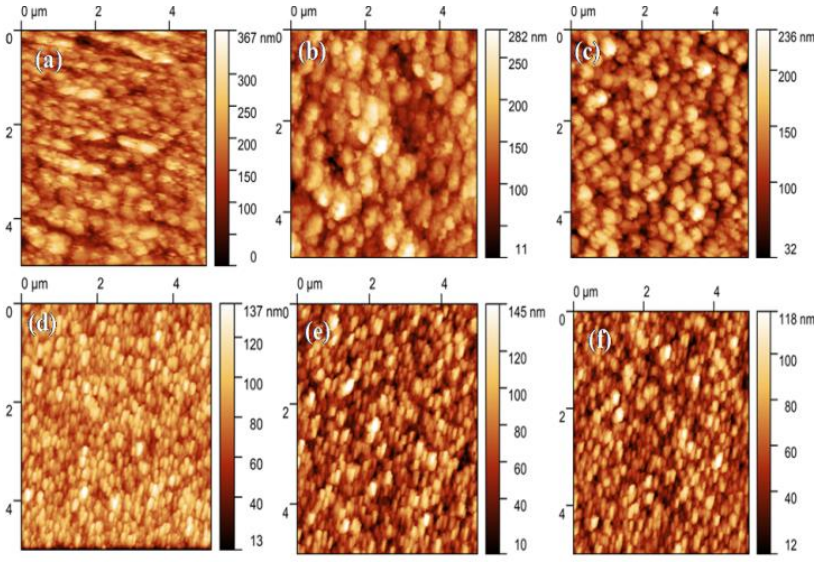

Fig. 7- Surface morphology through AFM image of bilayer thin films (a) annealed 323 K (b) annealed at 423 K and (c) annealed at 523 K and multilayer thin films (d) annealed 323 K (e) annealed at 423 K and (f) annealed at 523 K.

33.43nm respectively. Similarly the average surface (S_a) of the multilayer thin films annealed at 323 K, 423 K and 523 K were 81.71nm, 66.77nm and 56.850nm and the root mean square roughness (S_q) were 15.76nm, 23.20nm and 17.52nm respectively. The average surface roughness of both the bilayer and multilayer thin films decreases with increase in annealing temperature. The root mean square roughness of the bilayer thin films also decreases with increase in the annealing temperature but in case of multilayer thin films the root mean square roughness increases and then decreases. The crystallite size and surface roughness of the bilayer and multilayer thin films annealed at various annealing temperature were listed in Table 1.

3.2. Thermoelectric Properties

The Seebeck coefficient and electrical conductivity of the bilayer and multilayer SnSe and Bi_2Te_3 thin films were simultaneously measured by the Seebeck coefficient measurement device with temperature as a function. The Seebeck coefficient of bilayer and multilayer thin films, are shown in Fig. 8 (a) and (b) respectively.The Seebeck coefficient measures negative, for all annealed bilayer thin films, indicating that the majority of the charge carriers are electrons. At room temperature, the hall coefficient of all annealed bilayer and multilayer thin films were negative, confirming the n-type charge carrier. The carrier concentration of the bilayer thin films annealed at 323 K, 423 K and 523 K were 2.14 x 1017 cm^{-3}, 1.58 x 1017 cm^{-3} and 1.21 x 1017 cm^{-3} respectively. Similarly, for the multilayer thin films annealed at 323 K, 423 K and 523 K were 2.16 x 1017 cm^{-3}, 1.8 x 1017 cm^{-3}, and 1.4 x 1017 cm^{-3} respectively. The seebeck coefficient also increases as the crystallinity of the thin film increases. As the temperature increases, the value of Seebeck coefficient also rises. The increase in the Seebeck coefficient of the annealed thin films could be attributed to decrease in the carrier concentration. The maximum Seebeck coefficient for bilayer thin films was -350 μV/K at 573 K for 523 K annealed film. In the case of multilayer SnSe/ Bi_2Te_3 thin films, the Seebeck coefficient decreases from positive to negative as the temperature increases. The maximum Seebeck value for multilayer thin films is -350 μV/K at 573 K for 523 K annealed film.

Fig. 8 (c) and (d) illustrate the electrical conductivity of both bilayer and multilayer SnSe/ Bi_2Te_3 thin films. The electrical conductivity of the bilayer SnSe/ Bi_2Te_3 thin films varies for different annealing temperatures. The electrical conductivity increases with increasing temperature for 323 K and 423 K annealed thin films, but for 523 K annealed thin films, the electrical conductivity decreases as the temperature increases. As a semiconductor, the electrical conductivity of all annealed bilayer and multilayer thin films has increased linearly with temperature. The increase in electrical conductivity could be attributed to a larger crystal size and better crystal orientation. Because conductivity is directly proportional to carrier concentration ($\sigma = ne\mu$), the drop in electrical conductivity of the 523 K annealed bilayer thin film is attributed to a decrease in carrier concentration [37]. For multilayer SnSe/ Bi_2Te_3 thin films, the electrical conductivity of 423 K and 523 K annealed thin films gradually rises as the temperature increases, but for 323 K annealed film, the electrical conductivity rises and then falls. The maximum electrical conductivity of 170 S/m at 573 K for 523 K-annealed multilayer thin film was achieved. The increase in the annealing temperature increases the electrical conductivity because of high of increase in mobility for high crystal orientation and increase in the crystallite size decreases the carrier concentration[38].

The Seebeck Coefficient and Electrical Conductivity can be used to compute the Power Factor ($PF = S^2\sigma$)[6]. The power factor determines the performance of the thermoelectric generator. The power factor of all the bilayer SnSe/ Bi_2Te_3 thin films annealed at various annealing temperatures increases as the temperature increases. The power factor of the bilayer and multilayer thin films at different annealing temperature were shown in Fig. 8 (e) and (f) respectively. The maximum power factor obtained was 25 W/K^2m at 573 K for 523 K annealed thin film. Similarly, the power factor of all the annealed multilayer thin films of SnSe and Bi_2Te_3 increases. The power factor of SnSe/ Bi_2Te_3 multilayer thin film annealed at 323 K gives the least values; this was due to the poor electrical conductivity of the particular thin film. Maximum power factor of 18 W/K^2m is achieved for the 523 K annealed film at 573 K.

The total thermal conductivity ($k = k_e + k_l$) is the sum of the electrical and lattice thermal conductivities. The electrical thermal conductivity (k_e) is directly proportional to the electrical conductivity which was stated by Weidemann Franz law: $k_e = L\sigma T$, where L is the Lorentz number and it is 2.45 x 10-8 W/K^{-2} [30]. As the electrical conductivity increases, the electrical thermal conductivity also

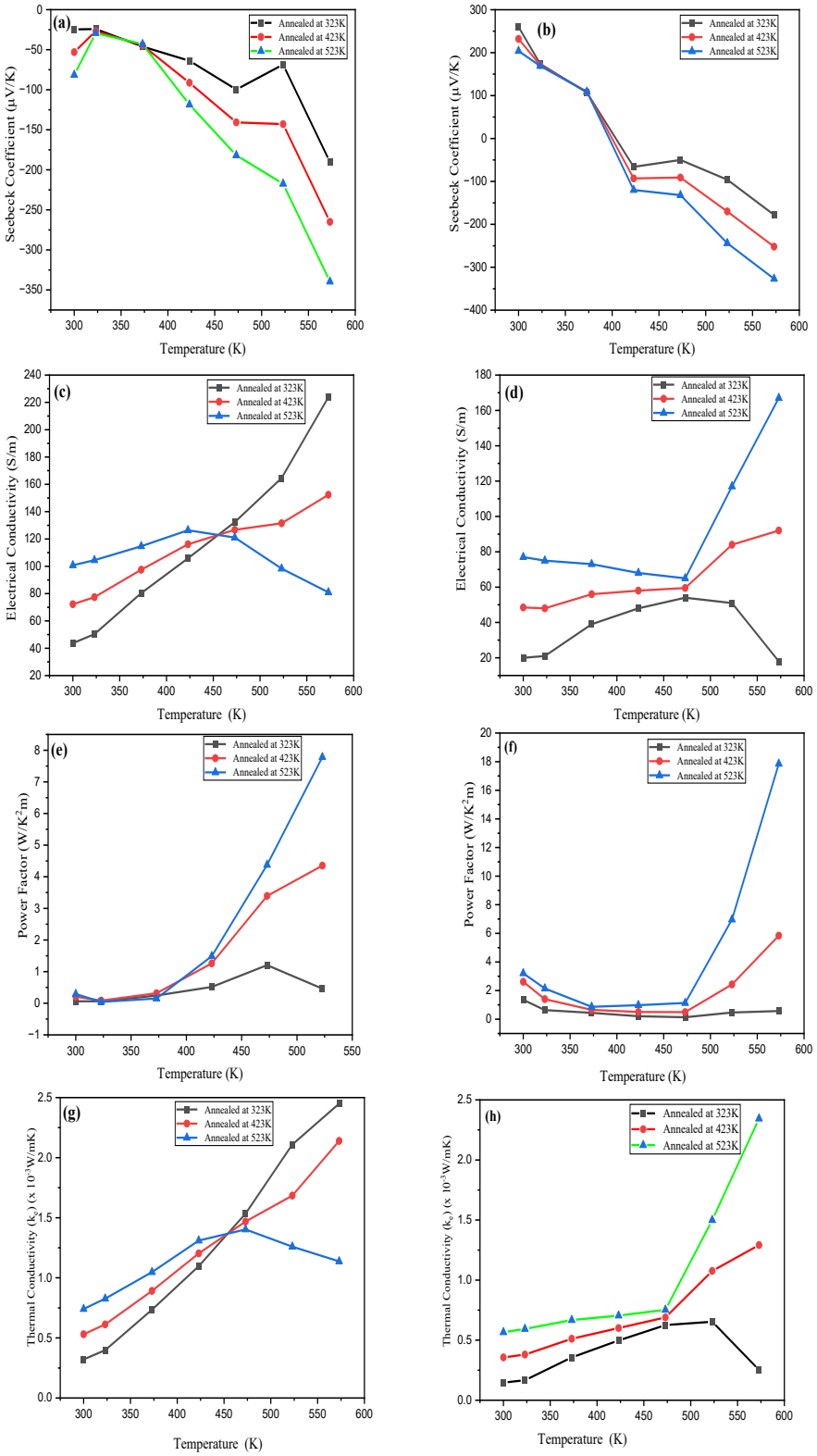

Fig. 8- Seebeck Coefficient of (a) bilayer (b) multilayer. Electrical Conductivity of (c) Bilayer (d) Multilayer. Power Factor of (e) Bilayer (f) Multilayer. Electrical thermal Conductivity of (g) Bilayer and (h) Multilayer.

increases. As a measure to decrease the electrical thermal conductivity, it reduces the electrical conductivity of the thermoelectric materials. In semiconductors, more than 90% of the total thermal conductivity is due to the lattice thermal conductivity [39]. The electrical thermal conductivity of the bilayer and multilayer thin films annealed at various annealing temperature were shown in Fig. 8 (g) and (h). The maximum electrical and thermal conductivity for bilayer thin film was 2.48 W/mK at 573 K for 323 K annealed thin film. The 523 K-annealed bilayer thin film shows poor electrical and thermal conductivity. In the case of multilayer thin films, the maximum electrical thermal conductivity obtained was 18 W/mK at 523 K for annealed thin film.

4. Conclusions

The bilayer and multilayer SnSe/ Bi_2Te_3 were deposited on a glass substrate. After deposition, the films were given a post-annealing treatment at 323 K, 423 K, and 523 K for 30 minutes. The structure and morphology of all the annealed thin films were investigated by XRD, SEM, and FESEM [24]. The thermoelectric properties of the bilayer and multilayer thin films annealed at various temperatures were studied. All the annealed films of the bilayer and multilayer thin films show a rise in Seebeck coefficient value as the temperature increases. Both the bilayer and multilayer thin films annealed at 523 K gives the highest Seebeck Coefficient of -350 μV/K at 573 K. Since total thermal conductivity of the samples was not found, ZT value was not calculated. As the Seebeck coefficient value of the 523 K annealed film increases, the power factor of that film increases. In most of the cases Power Factor determines the performance of the thermoelectric Performance. The highest Power Factor achieved by bilayer and multilayer thin films was 25 W/ K^2m and 18 W/ K^2m at 573 K. From both SnSe/ Bi_2Te_3 bilayer and multilayer thin films annealed at various temperatures, the films annealed at 523 K show better performance which is suitable for mid temperature thermoelectricity generation, particularly in applications where temperature gradients are present, such as in automotive or industrial processes. It is also suitable for refrigeration and air conditioning. The mechanical adaptability of multilayer thin films makes them ideal for incorporation into flexible and wearable electronic systems, where thermoelectric materials can be used for both energy harvesting and temperature regulation.

5. Declaration

5.1. Ethical Approval

Not applicable since no human or animal studies were done.

5.2. Competing Interests

The authors declare no conflict of interests.

5.3. Funding

This research received no external funding.

5.4. Availability of Data and Material

Not applicable since no datasets were used in this research.

References

1. Gayner C, Kar KK, Kim W. Recent progress and futuristic development of PbSe thermoelectric materials and devices. Materials Today Energy. 2018;9:359-76..
2. García VM, Nair PK, Nair MTS. Copper selenide thin films by chemical bath deposition. Journal of Crystal Growth. 1999;203(1-2):113-24.
3. Lin J-M, Chen Y-C, Yang C-F, Chen W. Effect of Substrate Temperature on the Thermoelectric Properties of the Sb_2Te_3 Thin Films Deposition by Using Thermal Evaporation Method. Journal of Nanomaterials. 2015;2015:1-6.
4. Dughaish ZH. Lead telluride as a thermoelectric material for thermoelectric power generation. Physica B: Condensed Matter. 2002;322(1-2):205-23.
5. Morgan KA, Tang T, Zeimpekis I, Ravagli A, Craig C, Yao J, et al. High-throughput physical vapour deposition flexible thermoelectric generators. Sci Rep. 2019;9(1):4393-.
6. Navone C, Soulier M, Plissonnier M, Seiler AL. Development of (Bi,Sb)2(Te,Se)3-Based Thermoelectric Modules by a Screen-Printing Process. Journal of Electronic Materials. 2010;39(9):1755-9.
7. Fan P, Zhang P-c, Liang G-x, Li F, Chen Y-x, Luo J-t, et al. High-performance bismuth telluride thermoelectric thin films fabricated by using the two-step single-source thermal evaporation. Journal of Alloys and Compounds. 2020;819:153027.
8. Han M-K, Jin Y, Lee D-H, Kim S-J. Thermoelectric Properties of Bi_2Te_3: CuI and the Effect of Its Doping with Pb Atoms. Materials (Basel). 2017;10(11):1235.
9. Ju H, Kim M, Park D, Kim J. A Strategy for Low Thermal Conductivity and Enhanced Thermoelectric Performance in SnSe: Porous SnSe1-xSx Nanosheets. Chemistry of Materials. 2017;29(7):3228-36.
10. Inayat SB, Hussain MM. Power generation from thermoelectric system-embedded Plexiglas for green building technology. Applied Nanoscience. 2012;3(4):335-42.
11. Beretta D, Neophytou N, Hodges JM, Kanatzidis MG, Narducci D, Martin- Gonzalez M, et al. Thermoelectrics: From history, a window to the future. Materials Science and Engineering: R: Reports. 2019;138:100501.
12. Takashiri M, Shirakawa T, Miyazaki K, Tsukamoto H. Fabrication and characterization of bismuth-telluride-based alloy thin film thermoelectric generators by flash evaporation meth-

od. *Sensors Actuators, A Phys* 2007; 138 (2):329–34.
13. Han C, Li Z, Dou S. Recent progress in thermoelectric materials. Chinese Science Bulletin. 2014;59(18):2073-91.
14. Klochko NP, Kopach VR, Tyukhov II, Khrypunov GS, Korsun VE, Nikitin VO, et al. Wet chemical synthesis of nanostructured semiconductor layers for thin-film solar thermoelectric generator. Solar Energy. 2017;157:657-66.
15. Li D, Gong Y, Chen Y, *et al. Recent Progress of Two-Dimensional Thermoelectric Materials*., 2020.
16. Zhao LD, Lo SH, Zhang Y, *et al.* Ultralow thermal conductivity and high thermoelectric Fig. of merit in SnSe crystals. *Nature* 2014; 508 (7496):373–7.
17. Wang Y, Shi Y, Mei D, Chen Z. Wearable thermoelectric generator to harvest body heat for powering a miniaturized accelerometer. Applied Energy. 2018;215:690-8.
18. Saleemi M, Toprak MS, Li S, Johnsson M, Muhammed M. Synthesis, processing, and thermoelectric properties of bulk nanostructured bismuth telluride (Bi_2Te_3). J Mater Chem. 2012;22(2):725-30.
19. Chen Z-G, Han G, Yang L, Cheng L, Zou J. Nanostructured thermoelectric materials: Current research and future challenge. Progress in Natural Science: Materials International. 2012;22(6):535-49.
20. Chandra S, Banik A, Biswas K. -nType Ultrathin Few-Layer Nanosheets of Bi-Doped SnSe: Synthesis and Thermoelectric Properties. ACS Energy Letters. 2018;3(5):1153-8.
21. Ju H, Kim M, Yang J, Kim J. Te Nanoneedles Induced Entanglement and Thermoelectric Improvement of SnSe. Materials (Basel). 2020;13(11):2523.
22. Chen Z-G, Shi X, Zhao L-D, Zou J. High-performance SnSe thermoelectric materials: Progress and future challenge. Progress in Materials Science. 2018;97:283-346.
23. Kim I-H. (Bi,Sb)2(Te,Se)3-based thin film thermoelectric generators. Materials Letters. 2000;43(5-6):221-4.
24. Goldsmid HJ. Bismuth telluride and its alloys as materials for thermoelectric generation. *Materials (Basel)* 2014; 7 (4):2577–92.
25. Cai S, Hao S, Luo Y, Su X, Luo Z-Z, Hu X, et al. Ultralow Thermal Conductivity and Thermoelectric Properties of Rb-$_2Bi_8Se_{13}$. Chemistry of Materials. 2020;32(8):3561-9.
26. Zheng ZH, Fan P, Luo JT, *et al.* Thermoelectric properties of bismuth antimony tellurium thin films through bilayer annealing prepared by ion beam sputtering deposition. *Thin Solid Films* 2014; 562:181–4.
27. Mozetič M. Surface Modification to Improve Properties of Materials. Materials (Basel). 2019;12(3):441.
28. Song L, Zhang J, Iversen BB. Enhanced thermoelectric properties of SnSe thin films grown by single-target magnetron sputtering. Journal of Materials Chemistry A. 2019;7(30):17981-6.
29. Matsuoka K, Okuhata M, Hatsuta N, Takashiri M. Effect of composition on the properties of bismuth telluride thin films produced by galvanostatic electrodeposition. Transactions of the Materials Research Society of Japan. 2015;40(4):383-7.
30. Gong X, Feng M, Wu H, Zhou H, Suen C, Zou H, et al. Highly (100)-orientated SnSe thin films deposited by pulsed-laser deposition. Applied Surface Science. 2021;535:147694.
31. Rajesh S, Parvathi MM, Mohan A, Arivazhagan V. Preparation and characterization of vacuum evaporated SnSe and SnSe2 multilayer thin films. AIP Conference Proceedings: AIP; 2012.
32. Singh NK, Bathula S, Gahtori B, Tyagi K, Haranath D, Dhar A. The effect of doping on thermoelectric performance of p-type SnSe: Promising thermoelectric material. Journal of Alloys and Compounds. 2016;668:152-8.
33. Burton MR, Boyle CA, Liu T, McGettrick J, Nandhakumar I, Fenwick O, Carnie MJ. Full Thermoelectric Characterization of Stoichiometric Electrodeposited Thin Film Tin Selenide (SnSe). ACS Applied Materials & Interfaces. 2020;12(25):28232-8.
34. Kwon S-D, Ju B-k, Yoon S-J, Kim J-S. Fabrication of Bismuth Telluride-Based Alloy Thin Film Thermoelectric Devices Grown by Metal Organic Chemical Vapor Deposition. Journal of Electronic Materials. 2009;38(7):920-4.
35. Kulsi C, Kargupta K, Ganguly S, Banerjee D. Enhanced thermoelectric performance of n-type bismuth selenide doped with nickel. Current Applied Physics. 2017;17(12):1609-15.
36. Yevdokymenko VY, Dobrozhan O, Pshenychnyi R, Opanasyuk A, Gnatenko Y, Bukivskii A, et al. The effect of annealing treatment on the structural and optical properties of nanostructured CuxO films obtained by 3D printing. Materials Science in Semiconductor Processing. 2023;161:107472.
37. Wang W ting, Zheng Z hao, Li F, *et al.* Synthesis process and thermoelectric properties of n-type tin selenide thin films. *J Alloys Compd* 2018; 763:960–5.
38. Takayama K, Takashiri M. Multi-layered-stack thermoelectric generators using p-type Sb_2Te_3 and n-type Bi_2Te_3 thin films by radio-frequency magnetron sputtering. Vacuum. 2017;144:164-71.
39. Mori R, Kurokawa T, Yamauchi K, Tanaka S, Takashiri M. Improved thermoelectric performances of nanocrystalline Sb_2Te_3/Cr bilayers by reducing thermal conductivity in the grain boundaries and heterostructure interface. *Vacuum* 2019; 161:92–7.